Site-specific ^{13}C NMR study on the locally distorted triangular lattice of the organic conductor κ-(BEDT-TTF)$_2$Cu$_2$(CN)$_3$

Y. Saito,[*] T. Minamidate, A. Kawamoto,[†] N. Matsunaga, and K. Nomura

Department of Physics, Hokkaido University, Sapporo 060-0810, Japan

To verify the effect of geometrical frustration, we artificially distort the triangular lattice of the quasi-two-dimensional organic conductor κ-(BEDT-TTF)$_2$Cu$_2$(CN)$_3$ [BEDT-TTF: bis(ethylenedithio)tetrathiafulvalene] by analogous-molecular substitution and apply ^{13}C NMR of bulk and substituted sites, electric conductivity, and static magnetic susceptibility measurements. The results indicate that the magnetic characteristics of the substituted sample are quantitatively similar to those of the pure sample. Moreover, the magnetic characteristics at the substituted sites are also the same as in the bulk. These results suggest that the observed magnetic properties may not be due to the geometrical frustration but the importance of disorder.

I. INTRODUCTION

κ-(BEDT-TTF)$_2X$ salts are well-known organic conductors based on bis(ethylenedithio)tetrathiafulvalene (BEDT-TTF) molecules which form dimers in the conduction layer. The compound X^- is a monovalent anion, so the formal charge of BEDT-TTF is $+0.5$. Although this is regarded as a quarter-filled system, the electronic state of κ-(BEDT-TTF)$_2X$ is believed to be half-filled due to the dimerization of the BEDT-TTF molecules [1].

At ambient pressure, the ground state of κ-(BEDT-TTF)$_2$Cu$_2$(CN)$_3$ [hereafter abbreviated as the (CN)$_3$ salt] is expected to be antiferromagnetic (AF) because its ratio of U/W is greater than that for κ-(BEDT-TTF)$_2$Cu[N(CN)$_2$]Cl [hereafter abbreviated as the Cl salt] [2], where U is the effective onsite Coulomb repulsion and W is the bandwidth, respectively. Contrary to the expectation, the (CN)$_3$ salt exhibits no magnetic ordering [3]. One possible reason no-AF ordering occurs in the (CN)$_3$ salt is the contribution of geometrical frustration of spins [3]. From density functional theory, we know that at room temperature, the ratio of interdimer transfer integrals $t'/t = 0.83$ is close to unity [4–6], where t is the nearest-neighbor transfer and t' is the second-nearest-neighbor transfer, respectively. Moreover, the exchange interaction, $J(t) = -2t^2/U$, the ratio of $J(t')/J(t)$, is close to unity, suggesting a nearly isotropic triangular lattice with $S = 1/2$. In this case, AF ordering could be suppressed by the geometrical frustration of the spins, which is called a resonating valence bond (RVB) state [7]. However, optical conductivity measurements of the (CN)$_3$ salt do not reveal a clear-cut energy gap at all temperatures [8,9], which is expected from a Mott insulator due to the concomitant large U/W. Moreover, charge instability below 60 K was reported in the (CN)$_3$ salt by ^{13}C nuclear magnetic resonance (NMR) [10,11] and Raman spectroscopy [12].

In recent years, studies about introducing random potential [13–15] or random exchange interaction [16,17] to a Mott insulator have been proceeded. Disorder or randomness is a source of localization in strongly correlated electron systems. In this case, conduction electrons localize by impurity scattering to form an *Anderson insulator*. Contrary to a Mott insulator, no gap appears at the Fermi surface in Anderson insulators. Some theories predict that a soft Hubbard gap, whose density of state with zero density of states at $E_{\rm F}$, emerges by introducing disorder to the strongly correlated electron system [13–15]. Due to competition between electron correlation and randomness, a Mott-Anderson transition is expected and long-range magnetic ordering might be suppressed if the extent of disorder exceeds over critical value.

Another aspect of the disorder effect is the inhomogeneity of exchange interactions: the random potential would make electrons inhomogeneous and give rise to the modulation of exchange couplings among spins. An exact diagonalization calculation in the triangular-lattice system shows that a magnetic ordering state is suppressed by the presence of randomness in the nearest-neighbor interactions, where the electronic state is not the RVB state but rather an Anderson-like localized spin singlet state called a random spin singlet state or a valence-bond glass state [16]. The numerical calculation reproduces experimental results, including T-linear low-temperature specific heat [18] and the power-law temperature dependence of the NMR spin-lattice relaxation rate [19].

To investigate the disorder effects of the Mott-insulating state of κ-(BEDT-TTF) salts, the Cl salt was irradiated by x-ray, which introduces disorder and changes the Mott-insulating state of the Cl salt into a soft-Hubbard-gapped insulating state [20] and, simultaneously, AF ordering disappears [21]. Recently, the disorder in the anion groups has been suggested to act on the BEDT-TTF layers via hydrogen bonds, whereby the charge distribution is altered and domain boundaries appear in the (CN)$_3$ salt [22,23]. Therefore, in the Mott-Anderson or in the vicinity of that state, the disorder-induced nonmagnetic state may be realized and the

————————
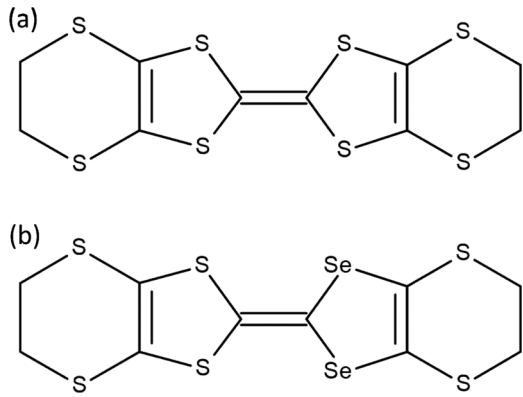[*]sai10@phys.sci.hokudai.ac.jp
[†]atkawa@phys.sci.hokudai.ac.jp

FIG. 1. Molecular structures of (a) BEDT-TTF and (b) us-BEDT-STF. One side of the central C=C bond in BEDT-TTF and that of the central C=C bond far from Se atoms in BEDT-STF are enriched with the ^{13}C isotope for NMR experiments.

relationship between the physical properties and disorder in the $(CN)_3$ salt is of significant research interest.

Experimental observations in the $(CN)_3$ salt have been explained through triangular-lattice or disordered-state models. Therefore, experimental verification is required to determine whether the observed behavior is due to the geometrical frustration of the spins in the triangular lattice or to a disordered state. One approach is to artificially distort triangular lattices.

Note that x-ray irradiation mainly affects the crystal surface owing to the large x-ray absorption coefficient $\mu = 108 \text{ cm}^{-1}$ for Cu $K\alpha$ radiation and produces free radicals on the surface in the $(CN)_3$ salt. Therefore, this technique is not suited for investigating the magnetic properties. Moreover, it is unclear whether x-ray irradiation and anion disorder via hydrogen bonding in pure samples introduces disorder in the conduction plane. An alternative approach is analogous-molecular substitution to directly introduce disorder into the conduction layer, which is the method we use herein. Specifically, we focus on a unsymmetrical (us-) bis(ethylenedithio)diselenadithiafulvalene (BEDT-STF), wherein one side of the S in the central ring of the TTF skeleton is replaced with Se atoms [see Fig. 1(b)]. The advantages of substituting BEDT-STF for BEDT-TTF are that (i) structural distortion is minimized because BEDT-TTF and BEDT-STF have almost the same molecular structure, (ii) the large spread of Se 4d orbital creates sufficient disorder to affect the intermolecular transfer integrals, and (iii) the substitution fraction and uniformity can be determined by elemental analysis to detect the Se atoms, which exist only at substituted sites. However, the primary important advantage is that the transfer integrals around the BEDT-STF molecule are modified by the Se orbitals, which locally distorts the triangular lattice.

NMR is a microscopic probe that measures the static and dynamic magnetic properties. The local spin susceptibility can be determined from the Knight shift K and magnetic fluctuations from the spin-lattice relaxation rate T_1^{-1}. Many previous NMR studies of BEDT-TTF salts have contributed important information on these salts [24,25]. By suppressing the frustration, some change of magnetic behavior is expected because spin susceptibility or the spin-lattice relaxation rate

involves the frustration effect in the RVB state. Herein, to elucidate the magnetic properties of the $(CN)_3$ salt, we apply ^{13}C NMR to bulk BEDT-TTF sites and compare the NMR results of pure samples with those of BEDT-STF–substituted samples. Moreover, it is expected that impurity sites behave differently from bulk sites, as the local impurities induce staggered moments near the center of disorder in the vicinity of antiferromagnetic compounds [26,27]. However, few NMR studies of impurity sites exist. To address this void, we replaced nonenriched BEDT-TTF with ^{13}C-enriched BEDT-STF so that ^{13}C-NMR targets the impurity sites.

II. EXPERIMENTAL

Single crystals of κ-[(BEDT-TTF)$_{1-x}$(BEDT-STF)$_x$]$_2$Cu$_2$(CN)$_3$ of various stoichiometry ($x = 0$, 0.05, and 0.06) were prepared by electrochemical oxidation [28]. Using energy-dispersive x-ray spectroscopy with κ-(BEDT-STF)$_2$Cu$_2$(CN)$_3$ as a reference, the impurity fraction x was determined by comparing the intensity of S atoms to that of Se atoms. Samples with $x = 0$ and 0.05 consisted of ^{13}C-enriched BEDT-TTF and nonenriched BEDT-STF, and a sample with $x = 0.06$ consisted of ^{13}C-enriched BEDT-STF and nonenriched BEDT-TTF. To avoid the Pake-doublet problem [29], one side of the central C=C bond in BEDT-TTF and that of the central C=C bond far from Se atoms in BEDT-STF are enriched with the ^{13}C isotope. ^{13}C-substituted molecules were prepared through cross coupling [30]. The dc conductivity was measured along the c axis from room temperature down to 40 K for the pure and $x = 0.05$ samples by the standard four-point probe technique. The dc magnetization was measured for polycrystalline samples as a function of temperature from 300 to 2 K in a 2-T magnetic field using a magnetometer that is based on a superconducting quantum interference device (SQUID). NMR experiments were performed for each single crystal in a 7-T magnetic field applied perpendicular to the conduction plane. The NMR spectra were obtained by the fast Fourier transformation of the spin-echo signal with a $\pi/2-\pi$ pulse sequence. The NMR shifts are given in ppm relative to tetramethylsilane. The nuclear spin-lattice relaxation rate T^{-1} was measured by the conventional saturation-recovery method. The NMR shifts and linewidths were determined by fitting peaks to a Lorentz function with least-squares method. The constraint condition with fixing the area ratio of two peaks to that obtained at high temperature was applied below 4.2 K for the pure sample and below 10 K for the $x = 0.05$ and 0.06 samples, respectively. The spin-spin relaxation rate T_2^{-1} is defined as the rate corresponding to Lorentz decay. Error bars represent a standard deviation.

III. RESULTS AND DISCUSSION

A. Modification of transfer integrals

We consider the modification of transfer integrals due to the extended 4d orbital of the Se atoms. The 5% BEDT-STF substitution shown in Fig. 1(b) modifies the transfer integrals of the affected sites as shown in Fig. 2. In fact, the transfer integral in the side-by-side direction of the BEDT molecules of α-(BEDT-STF)$_2$I$_3$ is 46.5% greater than that of
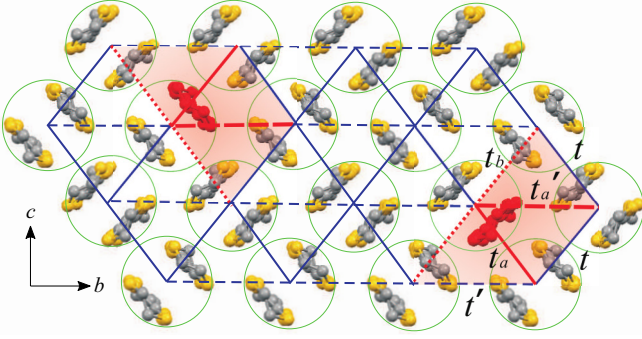
FIG. 2. Schematic view of BEDT-TTF dimers in the bc plane. Red molecules represent BEDT-STF molecules. Original nearly isotropic and modified triangular lattices are shown by blue and red lines, respectively, where t and t' are the original transfer integrals and t_a, t_a', and t_b are the transfer integrals around the BEDT-STF molecule.

α-(BEDT-TTF)$_2$I$_3$ [31]. Because κ-type salts also have orthogonal molecular packing, a similar increase of the transfer integrals is expected in the (CN)$_3$ salt. Since the transfer integral consists of BEDT-TTF and BEDT-STF in the substituted system, the transfer integral should be around half of that consisting of BEDT-STF and BEDT-STF. Therefore, the interdimer transfer integrals around the substituted dimer may be estimated to be about 23% greater than that of the original dimer, making the J around the BEDT-STF molecule 1.5 times greater than the original J. As shown in Fig. 2, 20% of the triangular lattices are distorted in the $x = 0.05$ sample; thus, the resulting area of the original triangular lattice is confined to a radius of 2–3 dimers. To verify the effect of disorder, we measured the electrical conductivity and compared the results with those of previous reports.

B. Conductivity

Figure 3(a) shows conductivity normalized to the data at room temperature for $E \parallel c$ as a function of $T^{-1/3}$ for both samples. In the pure sample, the result is consistent qualitatively with that of previous reports [10,22], whereas the decrease of the conductivity near room temperature is suppressed in the $x = 0.05$ sample. The conductivities of both samples are fit by the nearest-neighbor-hopping (NNH) and variable-range-hopping (VRH) equations,

$$\sigma(T) \propto \exp(-\Delta/T), \tag{1}$$

$$\sigma(T) \propto \exp[(-T_0/T)^{1/(d+1)}], \tag{2}$$

where Δ is the activation energy for the NNH model, T_0 is the activation energy for the VRH model, $d = 2$ is expected in two-dimensional VRH, $d = 1$ is known to appear due to the long-range Coulomb interaction proposed by Efros and Shklovskii (ES), and T_{cross} is the crossover temperature from the NNH model in the high-temperature region to the VRH model in the low-temperature region. For the pure sample, the conductivity can be fit by the NNH model above T_{cross} in the inset of Fig. 3(a), whereas the VRH model with $d = 2$ is suitable below T_{cross}, as shown in Fig. 3(a). The fitting
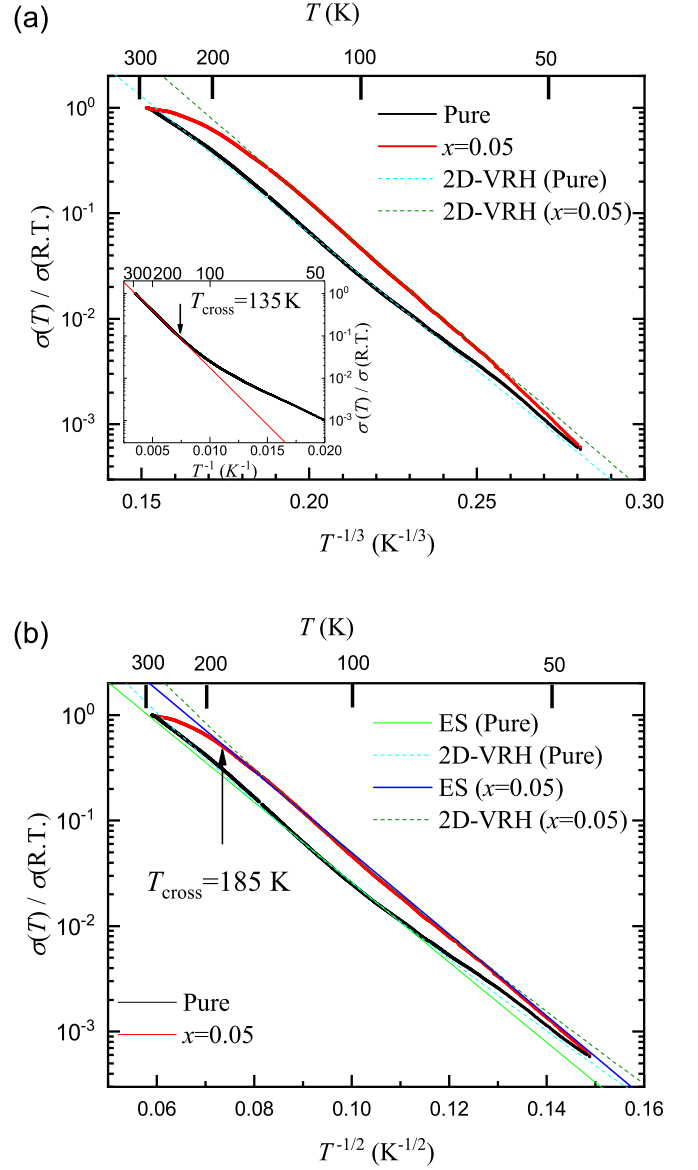

FIG. 3. Normalized conductivity of pure and $x = 0.05$ samples as a function of (a) $T^{-1/3}$ and (b) $T^{-1/3}$. The solid (dashed) line shows the fit given by the ES (2D-VRH) model. Inset in (a) shows Arrhenius plot of the pure sample and the solid line shows the fit given by the NNH model.

parameters are given in Table I. For the $x = 0.05$ sample, the VRH model fit with $d = 2$ deviates at low temperature in Fig. 3(a), while the ES model gives a better fit as shown in Fig. 3(b), although the ES model for the pure sample does not follow its conductivity.

TABLE I. Transport parameters.

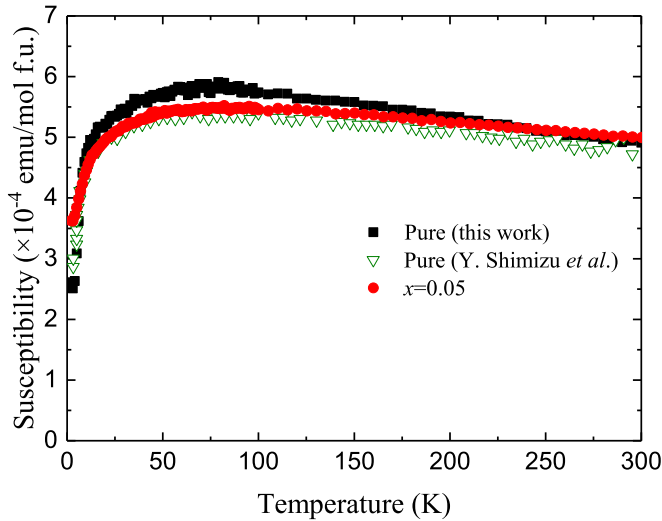|	Pure sample	$x = 0.05$ sample
Δ (K)	620	N/A
T_0 (eV)	18.3 (2D-VRH)	0.68 (ES)
T_{cross} (K)	135	185

FIG. 4. Magnetic susceptibility as a function of temperature for pure and $x = 0.05$ samples. The data of one of the pure samples indicated by the inverted triangle are taken from Ref. [3].

Conductivity above T_{cross} significantly differs between the pure and $x = 0.05$ samples. For the $x = 0.05$ sample, the temperature dependence of conductivity does not change much above T_{cross}. Although the temperature dependence of the conductivity was fit by the NNH model, the obtained value of Δ is too small to explain the crossover from the NNH to VRH model.

Infrared spectroscopy measurements for the pure and $x = 0.04$ samples were also performed to confirm the substitution effect. The spectral weight of the $x = 0.04$ sample shifted from high to low frequency compared with that of the pure sample, and this behavior was enhanced with decreasing temperature (the data are not shown here), indicating the substitution affected the electronic state of the pure sample. These results demonstrate that the substitution enhances conduction and increases T_{cross} above that of the pure sample. As BEDT-STF substitution does not introduce carriers, we must rule out any effect due to carrier doping. To explain the results for the ES behavior and the $x = 0.05$ sample, we suggest that competition between electron correlations and randomness possibly play a role [15] and further detailed study could be needed. For both samples, the fit suggests that no intrinsic energy gap opens, and the substitution effect was confirmed by studying the transport properties of the $x = 0.05$ sample.

C. Static magnetic susceptibility

The static magnetic susceptibility of the pure and $x = 0.05$ samples are shown in Fig. 4, along with the result of previous work [3]. In this figure, the core diamagnetic contribution of -4.37×10^{-4} emu/mol f.u. [3] is already subtracted. For the $x = 0.05$ sample, the temperature dependence is quantitatively fairly similar to that of the pure sample; both exhibit a hump at around 60 K and rapidly decrease below 20 K. The value of $\chi = 5 \times 10^{-4}$ emu/mol f.u. at 300 K is greater than that found for other κ salts, i.e., $\chi = 4.5 \times 10^{-4}$ emu/mol f.u. [32]. The static susceptibility remains essentially unchanged on distortion of the triangular lattice.
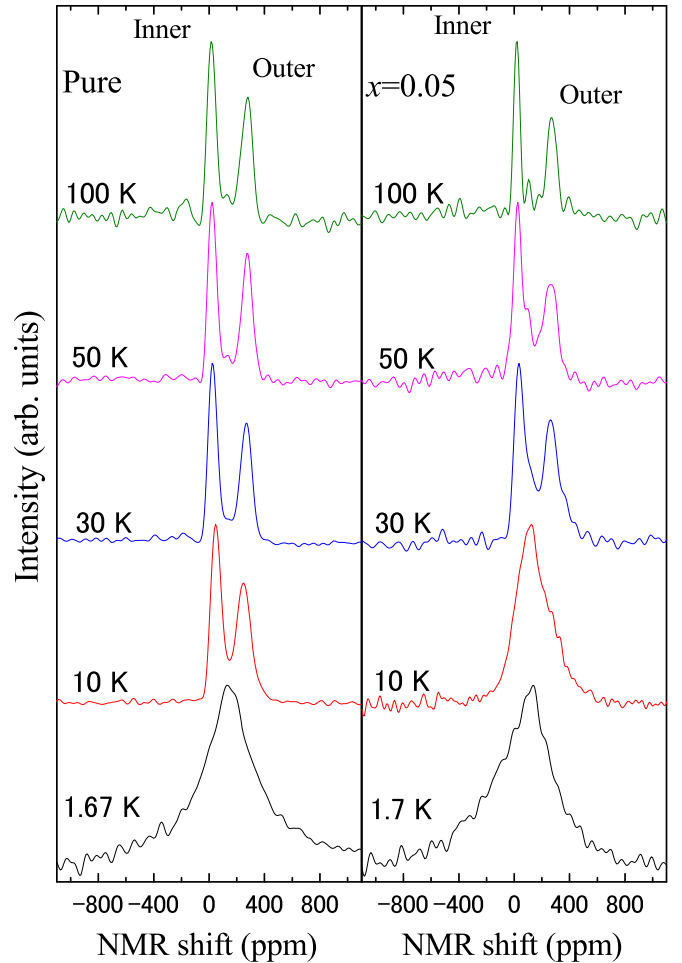

FIG. 5. NMR spectra at several temperatures in a field of $H\|a^*$. Left (right) panel shows the results for the pure ($x = 0.05$) sample.

D. NMR spectra, line shift, and linewidth

Figure 5 shows the NMR spectra at several temperatures for a magnetic field perpendicular to the conduction plane ($H\|a^*$). The left (right) panel shows the results for the pure ($x = 0.05$) sample. Two peaks corresponding to the inner and outer sites [19,33] appear in both spectra. For both samples, linewidth broadens with decreasing temperature and no AF ordering appears, which is consistent with the previous reports for the pure material [10,19].

Figure 6 shows how the NMR lines shift with temperature. Both samples showed similar line shifts that were proportional to the spin susceptibility. We obtain the hyperfine coupling constants from the $\delta - \chi$ plot (see Fig. 7). Table II summarizes the hyperfine coupling constants, which are almost the same for both samples. The hyperfine coupling constant of the inner site is negative, whereas that of the outer site is positive; this is consistent with other κ salts [33]. As shown in Fig. 4, the finite susceptibility at 0 K seems to remain at approximately half its value at room temperature, which is expected from a gapless spin liquid. Owing to slight paramagnetic impurities, the spin susceptibility depends on the subtraction of the paramagnetic impurities. NMR, however, can detect local spin susceptibility independent of paramagnetic impurities. The NMR shift δ is

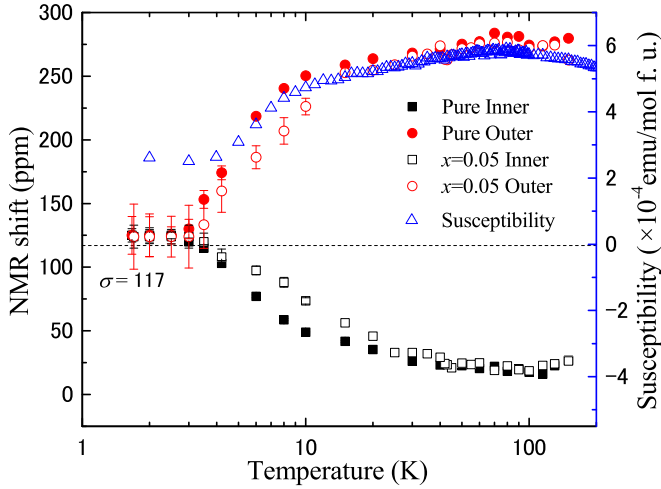FIG. 6. NMR line shift and magnetic susceptibility as a function of temperature.

written as

$$\delta = K + \sigma = A_{\text{hf}} \chi_s + \sigma, \qquad (3)$$

where K is the Knight shift, A_{hf} is the hyperfine coupling constant, and σ is the chemical shift. To discuss the spin susceptibility, the chemical shift was determined to be $\sigma = 117$ ppm from the chemical-shift tensor of $(\text{BEDT-TTF})^{+0.5}$ [34]. With decreasing temperature, the NMR shift approaches the chemical shift.

Figure 8 shows the temperature dependence of the FWHM of the NMR lines and the inset shows the temperature dependence of T_2^{-1} for the inner and outer sites of both samples. For Fourier transform NMR, the linewidth $\Delta\omega$ of the spectrum is generally described as

$$\Delta\omega = \frac{2\pi}{T_2} + \gamma_{\text{I}} \Delta H, \qquad (4)$$

where γ_{I} is the nuclear gyromagnetic ratio and ΔH is the inhomogeneity of the local magnetic field at the corresponding
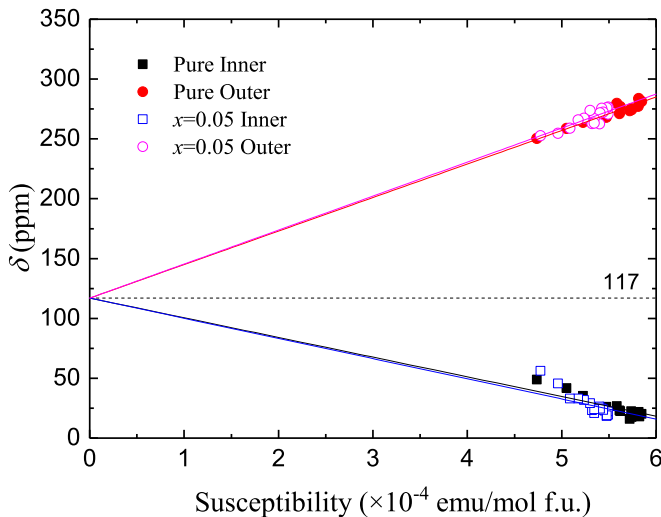
TABLE II. Hyperfine coupling constants.

	Value (kOe/μ_B)
$A_{\|a^*,\,\text{pure in}}$	−0.97
$A_{\|a^*,\,\text{pure out}}$	1.59
$A_{\|a^*,\,x=0.05\,\text{in}}$	−0.93
$A_{\|a^*,\,x=0.05\,\text{out}}$	1.56

nuclei. The first term is the inhomogeneous width caused by the dynamics and the second term is a static inhomogeneous width caused by the inhomogeneity of the external and local magnetic field. T_2^{-1} can detect slow magnetic fluctuations. In the pure sample, the NMR linewidth gradually broadens with decreasing temperature, whereas T_2^{-1} remains constant, indicating that the broadening is primarily to inhomogeneous broadening [19]. The outer site, which has a larger hyperfine coupling constant, has a broader NMR line than the inner site. Below 10 K, further broadening occurs. To determine the inhomogeneous linewidth ν, the natural linewidth of 2.8 kHz determined by T_2^{-1} is subtracted from the FWHM [see Eq. (4)]. The ratio of the inhomogeneous linewidth $\nu_{\text{out}}/\nu_{\text{in}}$ is approximately 2 from 60 K, where the linewidth starts to broaden, down to 10 K. This ratio is comparable to the analogous ratio of the hyperfine coupling constant $|A_{\text{out}}/A_{\text{in}}| = 1.64$. Thus, the linewidth broadening correlates with the hyperfine coupling constants, suggesting that the spin density on molecules is inhomogeneous. In other words, $\Delta K = A \Delta \chi$.

For the $x = 0.05$ sample, the line broadening is detected, which is greater than that for the pure sample from 60 to 15 K. As T_2^{-1} for the $x = 0.05$ sample is independent of temperature, the increase in linewidths is attributed to an enhanced static inhomogeneity, as for the pure sample. The ratio of the inhomogeneous NMR linewidth $\nu_{\text{out}}/\nu_{\text{in}} \simeq 2$ resembles that of the hyperfine coupling constant $|A_{\text{out}}/A_{\text{in}}| = 1.75$. This suggests the impurity substitution enhances the disorder.
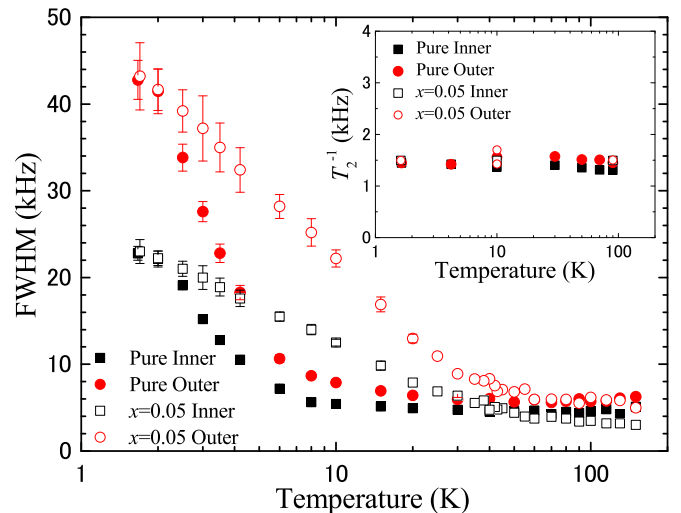

FIG. 7. Temperature dependence of $\delta - \chi$ plot.

FIG. 8. Temperature dependence of FWHM of NMR lines. Inset shows temperature dependence of T_2^{-1}.

Next, we focus on the anomalous increase of the FWHM of the NMR lines in the low-temperature region. The NMR linewidth of the spin singlet state is expected to be narrow. However, the FWHM does not decrease at low temperature. Recently, μSR measurements by Nakajima *et al.* suggested that spins paramagnetically fluctuate in zero magnetic field, and the microscopic phase separates into the singlet phase and the paramagnetic phase below 3 K [35]. To explain these results, Nakajima *et al.*, invoked microscopic paramagnetic islands surrounded by a singlet sea with a finite gap. As the volume fraction of the singlet sea is much greater than that of the paramagnetic area, the paramagnetic spin behaves as a magnetic impurity, contributing only to the linewidth as staggered magnetization. Thus, this singlet sea picture is consistent with the small Knight shift with a broad linewidth. Moreover, this single sea may be explained by the random-singlet model whose calculation shows the spin-liquid-like state on the triangular lattice with randomness [16]. Note that recently the existence of Dzyaloshinskii-Moriya interaction via spin-orbit coupling was suggested in the $(CN)_3$ salt [36], which might be also related to the broadening of the linewidth.

For the $x = 0.05$ sample, the FWHM also rapidly increases below 15 K. One possible explanation of this result is that the impurity substitution induces the AF moments; however, this can be ruled out because if impurities induce AF moments, the FWHM for $x = 0.05$ would be broader than that for the pure sample. However, the FWHM is almost the same for both samples at 1.7 K, in contrast to what happens above 15 K. Conversely, the paramagnetic island proposed by μSR [35] is independent of nonmagnetic impurities such as the BEDT-STF, so the paramagnetic islands are independent of the BEDT-STF impurities, resulting in a same-amplitude in-homogeneous field in both samples, and translating into the same broadening in both samples.

E. Nuclear spin-lattice relaxation rate

The nuclear spin-lattice relaxation rate $1/T_1$ probes spin fluctuation, which is written as

$$\frac{1}{T_1 T} = \frac{2\gamma_I^2 k_B}{(\gamma_e \hbar)^2} \sum_q (A_q A_{-q}) \frac{\chi_q''(\omega)}{\omega}. \quad (5)$$

Here, γ_e is the electron gyromagnetic ratio, A is the hyperfine coupling constants between the electron and nucleus, and $\chi_q''(\omega)$ is the imaginary part of the dynamic susceptibility at wave vector q. Figure 9 compares the temperature dependence of $(T_1 T)^{-1}$ of both samples with the result from a previous measurement of a double-^{13}C-enriched sample under the same magnetic field direction [19]. We determined T_1^{-1} by separately fitting a single exponential to the inner and outer sites, or by fitting the two exponential models to the sum of the spectral intensity below 20 K by using the ratio $T_{1,\text{inner}}/T_{1,\text{outer}} = 3$, which was determined at 100 K. This value is typical of κ-$(BEDT-TTF)_2 X$ salts. As temperature decreases, the quantity $(T_1 T)^{-1}$ increases and broadly peaks near 8 K. However, note that recovery curves for both samples deviate from the exponential fits below 6 K, which suggests distribution of T_1^{-1}. This distribution corresponds to the anomalous broadening below 8 K. Using $(T_1 T)^{-1}$ of the pure sample reproduces the results of previous work [19]. On the basis of the ratio U/W
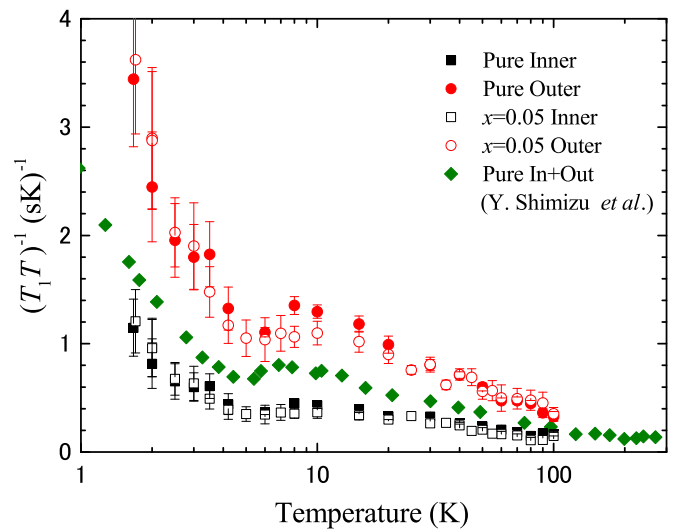

FIG. 9. Temperature dependence of $(T_1 T)^{-1}$ for the pure and $x = 0.05$ samples. The data of one of the pure samples indicated by the rhombus represents an average of the inner and outer sites and are taken from Ref. [19].

of the $(CN)_3$ salt, an AF transition temperature T_N comparable to that of the Cl salt is expected. The suppression of the AF transition indicates the characteristics of the geometrical frustration below the temperature $T_N = 27$ K [37] of the Cl salt. However, the temperature dependence of $(T_1 T)^{-1}$ for the $x = 0.05$ sample is quantitatively similar to that of the pure sample, indicating a lack of geometrical frustration. Another possibility is the impurity sites are bypassed, as a valence bond is formed from spins that are far apart [38]. We rule it out by the impurity-site NMR.

F. NMR of the impurity site

The impurity site in a locally magnetic correlated system is expected to behave differently than the bulk site. To verify geometrical frustration, applying NMR to the impurity sites provides useful information. However, NMR spectra affected by impurities has been discussed on the basis of using long tails of the spectrum line on the bulk site. Although using NMR to detect the impurity-site resonances is difficult in frustrated spin systems, we directly observed ^{13}C-NMR on impurity sites using ^{13}C-enriched BEDT-STF molecules.

Figure 10 shows NMR spectra from impurity sites at several temperatures. Two peaks are observed at 100 K. Linewidth broadening occurs at low temperature and no AF ordering appears. The NMR shift is less than that of the bulk sites. To estimate the local spin susceptibility of the impurity site, the hyperfine coupling constant of BEDT-STF is required. Therefore, we measured the magnetic susceptibility and NMR shift of the $x = 1$ sample so that we could obtain its hyperfine coupling constant for the same direction by $\delta - \chi$ plot. Figure 11 shows the $\delta - \chi$ plot for the $x = 1$ sample and the plot gives the hyperfine coupling constants $A_{\|a^*, x=1\,\text{in}} = -1.05$ kOe/μ_B and $A_{\|a^*, x=1\,\text{out}} = 1.48$ μ_B/kOe, and $\sigma = 110$ ppm. The hyperfine coupling constants of the $x = 1$ sample are very close to those of the pure sample, indicating the local spin susceptibility becomes small compared
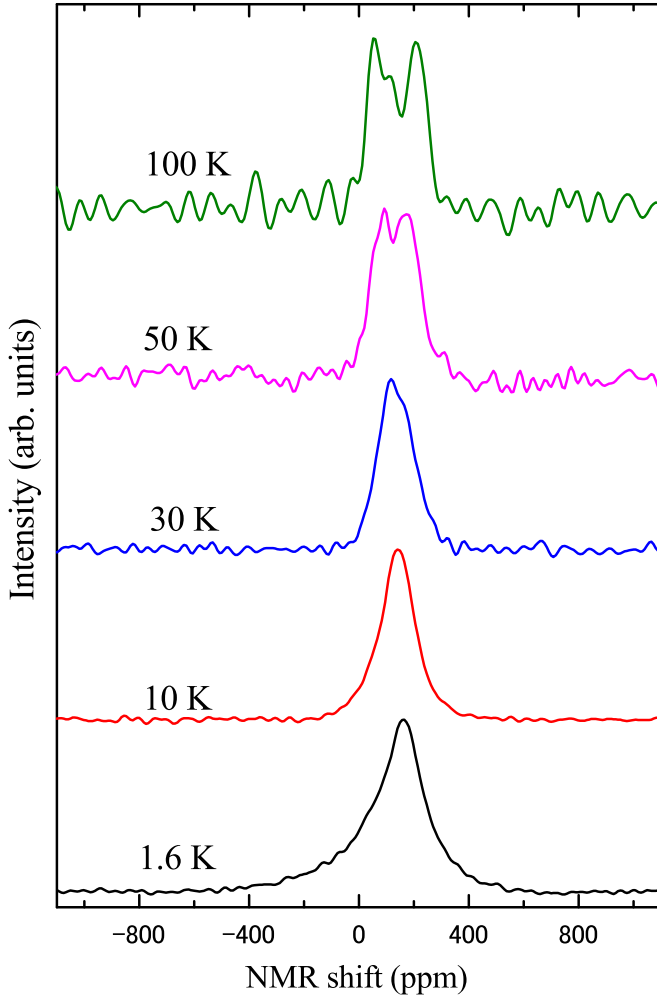
FIG. 10. NMR spectra of impurity sites at several temperatures.

FIG. 11. Temperature dependence of $\delta - \chi$ plot for the $x = 1$ sample.

$\chi_{imp} \simeq 0.6\chi_{bulk}$. Therefore, $\Delta\chi/\chi$ values at the bulk and impurity sites are much the same since $\nu \propto \Delta\chi$. These results suggest that impurities or defects do not induce staggered moments, but the staggered moments are induced in the whole crystal, which is consistent with the bulk-site results in Sec. III D. In the scenario of the linewidth broadening proposed as the Dzyaloshinskii-Moriya (DM) interaction through the spin-orbit coupling, the coupling of Se atoms is about five times greater than that of S atoms [36]. It may be expected that the staggered moments of the BEDT-STF site become several times greater than the BEDT-TTF site. However, experimental results are opposite. Therefore, further study is required to discuss the relation between the linewidth and the DM interaction. Instead, the scenario that paramagnetic spins are surrounded by a singlet sea in Sec. III D may be rather plausible.

with the pure sample. Also, the chemical shift of BEDT-STF is comparable to that of BEDT-TTF, indicating their chemical environments around ^{13}C are almost the same. To compare the spin susceptibility between BEDT-TTF and BEDT-STF sites without a chemical shift term, we used the following equation: $\Delta\delta = \delta_{out} - \delta_{in} = \Delta A\chi_{spin}$ [see Eq. (3)]. The local spin susceptibility at a BEDT-STF site, χ_{imp}, was estimated to be 60% of that at a BEDT-TTF site, χ_{bulk}, at 100 K where the NMR peak separation is clear. This reduction of the local spin susceptibility reveals the BEDT-STF substitution can affect the electronic state experimentally. The 60% spin susceptibility leads the magnetic moment of 0.8 μ_B in a dimer consisting of BEDT-TTF and BEDT-STF, suggesting the dimer-Mott insulating picture, i.e., 1 μ_B per dimer, is broken locally in the BEDT-STF-substituted system.

In frustrated spin systems, impurities can induce local staggered moments and line broadening is expected owing to staggered spin density oscillations, as expected from the AF character of magnetic correlations [26,27]. Figure 12 shows the temperature dependence of FWHM of the NMR lines from impurity sites as a function of temperature. The FWHM of the NMR line of the impurity site at low temperature is less than that of bulk sites. The ratio of inhomogeneous linewidth ν_{imp}/ν_{bulk} is about 0.5, which is consistent with

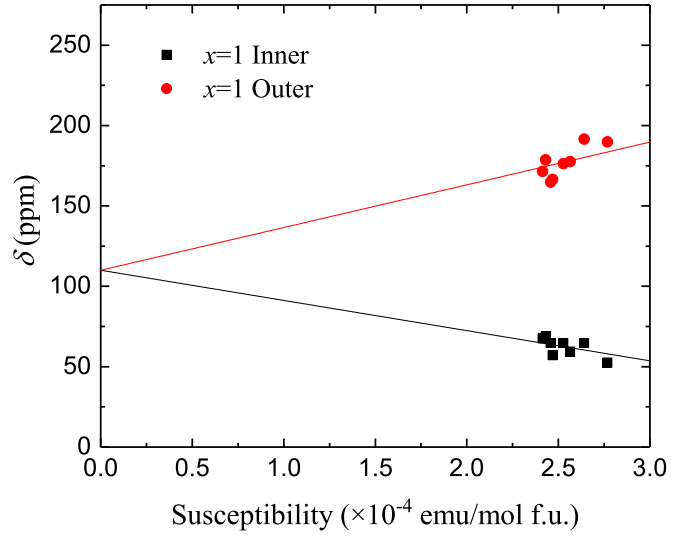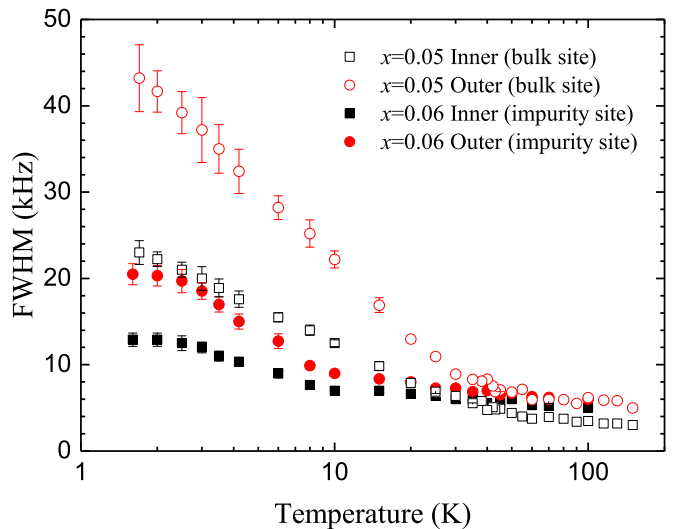FIG. 12. FWHM of NMR line for impurity and bulk sites as a function of temperature.
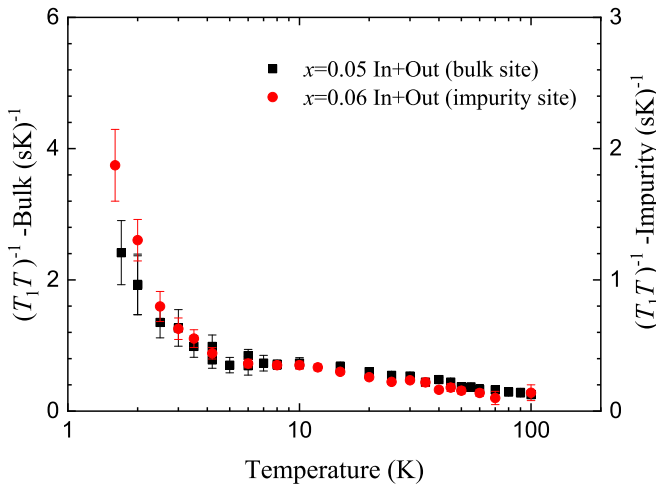
FIG. 13. Temperature dependence of the mean value of $(T_1T)^{-1}$ of the associated inner and outer sites for bulk and impurity sites. The results of the bulk site are plotted with the left axis, and the results of the impurity site are plotted with the right axis.

Figure 13 shows $(T_1T)^{-1}$ for the bulk and impurity sites, both as functions of temperature, where the right axis is multiplied by a factor of 2. Each curve is the mean value of the associated inner and outer sites. The temperature dependence of $(T_1T)^{-1}$ for the impurity site is similar to that for the bulk site. We also observed recovery curves deviated from the exponential fits below 8 K, which suggested distribution of T_1^{-1}. Scaling $(T_1T)^{-1}$ for impurity sites by a factor of 2 matches well with the results for $(T_1T)^{-1}$ for the bulk sites. In Fermi liquid theory, $(T_1T)^{-1}$ is proportional to the square of the product of the hyperfine coupling constant A_{hf} and the density of state $N(E_F)$ at the Fermi energy:

$$\frac{1}{T_1T} = \frac{\pi k_B}{\hbar} A_{\text{hf}}^2 N^2(E_F). \tag{6}$$

Here, $N(E_F)$ corresponds to the local spin susceptibility. Since χ_{imp} is $0.6\chi_{\text{bulk}}$, the $N^2(E_F)$ which was 2.77 ($= 1/0.6^2$) times smaller than that for the bulk site was expected. Therefore, the scaling factor of 2 should be explained by the small $N(E_F)$ at the impurity site.

The similar behaviors of $\Delta\chi/\chi$ and $(T_1T)^{-1}$ for both sites suggest that the electronic properties at the bulk and impurity sites are described by a one-fluid model. The result of the impurity site where the Mott insulating picture breaks being the same as that of the bulk site indicates that the magnetic behavior of the $(CN)_3$ salt is not due to long-range entanglement of the valence bond. Instead, the suppression of the AF transition and the electronic state of the $(CN)_3$ salt may be due to disorder and electronic correlation, in addition to the ideal geometrical frustration, as theoretically suggested [13–16].

IV. CONCLUSION

We investigated the conductivity and the magnetic properties of the $(CN)_3$ salt by artificially distorting its triangular lattice by substitution of BEDT-STF, which introduces disorder by modifying the transfer integrals among the BEDT-STF molecules.

The temperature dependence of conductivity of a sample with impurity fraction $x = 0.05$ does not change much above 200 K, indicating that the substitution enhances conductivity and leads to a crossover temperature T_{cross} that is greater than that of a pure sample. At low temperature, the conductivity of the $x = 0.05$ sample follows the ES model, which might be described by electronic correlation and randomness.

The NMR spectra reveal no magnetic ordering, and the spin susceptibility approaches the chemical shift below 3 K in both samples, which deviates from the magnetic susceptibility obtained by SQUID. From 60 to 15 K, the NMR linewidth of the $x = 0.05$ sample becomes broader than that of the pure sample, indicating the BEDT-STF substitution enhances disorder. The temperature dependence of $(T_1T)^{-1}$ for both samples is quantitatively similar. Moreover, the temperature dependence of $(T_1T)^{-1}$ for the impurity site where the Mott insulating picture breaks is similar to that of the bulk site, suggesting that the characteristics of $(T_1T)^{-1}$ are not due to geometrical frustration. NMR spectra from the impurity site suggest a decrease in local spin susceptibility and that no staggered moments are induced. Thus, the results indicate that the static and dynamic susceptibility do not change, even at temperatures 2 orders of magnitude less than the exchange interaction $J \simeq 250$ K. These results are in stark contrast to the expected effect of the substitution on conductivity. Thus, we suggest that the electronic state of the $(CN)_3$ salt is already the disordered system even in the pure sample, and that not only the ideal geometrical frustration but also the disorder effect should be considered.

[1] K. Kanoda, Phys. C Supercond. **282-287**, 299 (1997).

[2] T. Komatsu, N. Matsukawa, T. Inoue, and G. Saito, J. Phys. Soc. Jpn. **65**, 1340 (1996).

[3] Y. Shimizu, K. Miyagawa, K. Kanoda, M. Maesato, and G. Saito, Phys. Rev. Lett. **91**, 107001 (2003).

[4] H. C. Kandpal, I. Opahle, Y.-Z. Zhang, H. O. Jeschke, and R. Valentí, Phys. Rev. Lett. **103**, 067004 (2009).

[5] K. Nakamura, Y. Yoshimoto, T. Kosugi, R. Arita, and M. Imada, J. Phys. Soc. Jpn. **78**, 083710 (2009).

[6] H. O. Jeschke, M. de Souza, R. Valentí, R. S. Manna, M. Lang, and J. A. Schlueter, Phys. Rev. B **85**, 035125 (2012).

[7] P. Anderson, Mater. Res. Bull. **8**, 153 (1973).

[8] I. Kézsmárki, Y. Shimizu, G. Mihály, Y. Tokura, K. Kanoda, and G. Saito, Phys. Rev. B **74**, 201101 (2006).

[9] S. Elsässer, D. Wu, M. Dressel, and J. A. Schlueter, Phys. Rev. B **86**, 155150 (2012).

[10] A. Kawamoto, Y. Honma, and K. Kumagai, Phys. Rev. B **70**, 060510 (2004).

[11] A. Kawamoto, Y. Honma, K. Kumagai, N. Matsunaga, and K. Nomura, Phys. Rev. B **74**, 212508 (2006).

[12] K. Yakushi, K. Yamamoto, T. Yamamoto, Y. Saito, and A. Kawamoto, J. Phys. Soc. Jpn. **84**, 084711 (2015).

[13] K. Byczuk, W. Hofstetter, and D. Vollhardt, Phys. Rev. Lett. **94**, 056404 (2005).

[14] M.C.O. Aguiar, V. Dobrosavljević, E. Abrahams, and G. Kotliar, Phys. Rev. Lett. **102**, 156402 (2009).

[15] H. Shinaoka and M. Imada, J. Phys. Soc. Jpn. **78**, 094708 (2009).

[16] K. Watanabe, H. Kawamura, H. Nakano, and T. Sakai, J. Phys. Soc. Jpn. **83**, 034714 (2014).

[17] T. Shimokawa, K. Watanabe, and H. Kawamura, Phys. Rev. B **92**, 134407 (2015).

[18] S. Yamashita, Y. Nakazawa, M. Oguni, Y. Oshima, H. Nojiri, Y. Shimizu, K. Miyagawa, and K. Kanoda, Nat. Phys. **4**, 459 (2008).

[19] Y. Shimizu, K. Miyagawa, K. Kanoda, M. Maesato, and G. Saito, Phys. Rev. B **73**, 140407 (2006).

[20] T. Sasaki, Crystals **2**, 374 (2012).

[21] T. Furukawa, K. Miyagawa, T. Itou, M. Ito, H. Taniguchi, M. Saito, S. Iguchi, T. Sasaki, and K. Kanoda, Phys. Rev. Lett. **115**, 077001 (2015).

[22] M. Pinterić, M. Čulo, O. Milat, M. Basletić, B. Korin-Hamzić, E. Tafra, A. Hamzić, T. Ivek, T. Peterseim, K. Miyagawa, K. Kanoda, J. A. Schlueter, M. Dressel, and S. Tomić, Phys. Rev. B **90**, 195139 (2014).

[23] M. Dressel, P. Lazić, A. Pustogow, E. Zhukova, B. Gorshunov, J. A. Schlueter, O. Milat, B. Gumhalter, and S. Tomić, Phys. Rev. B **93**, 081201 (2016).

[24] F. Kagawa, K. Miyagawa, and K. Kanoda, Nat. Phys. **5**, 880 (2009).

[25] H. Mayaffre, S. Krämer, M. Horvatić, C. Berthier, K. Miyagawa, K. Kanoda, and V. F. Mitrović, Nat. Phys. **10**, 928 (2014).

[26] M. Takigawa, N. Motoyama, H. Eisaki, and S. Uchida, Phys. Rev. B **55**, 14129 (1997).

[27] N. Fujiwara, H. Yasuoka, Y. Fujishiro, M. Azuma, and M. Takano, Phys. Rev. Lett. **80**, 604 (1998).

[28] U. Geiser, H. H. Wang, K. D. Carlson, J. M. Williams, H. A. Charlier, J. E. Heindl, G. A. Yaconi, B. J. Love, M. W. Lathrop, J. E. Schirber, D. L. Overmyer, J. Ren, and M. Whangbo, Inorg. Chem. **30**, 2586 (1991).

[29] G. E. Pake, J. Chem. Phys. **16**, 327 (1948).

[30] S. Hirose, M. Misawa, and A. Kawamoto, Crystals **2**, 1034 (2012).

[31] M. Inokuchi, H. Tajima, A. Kobayashi, T. Ohta, H. Kuroda, R. Kato, T. Naito, and H. Kobayashi, Bull. Chem. Soc. Jpn. **68**, 547 (1995).

[32] A. Kawamoto, K. Miyagawa, Y. Nakazawa, and K. Kanoda, Phys. Rev. B **52**, 15522 (1995).

[33] Y. Saito and A. Kawamoto, Solid State Nucl. Magn. Reson. **73**, 22 (2016).

[34] T. Kawai and A. Kawamoto, J. Phys. Soc. Jpn. **78**, 074711 (2009).

[35] S. Nakajima, T. Suzuki, Y. Ishii, K. Ohishi, I. Watanabe, T. Goto, A. Oosawa, N. Yoneyama, N. Kobayashi, F. L. Pratt, and T. Sasaki, J. Phys. Soc. Jpn. **81**, 063706 (2012).

[36] S. M. Winter, K. Riedl, and R. Valentí, Phys. Rev. B **95**, 060404 (2017).

[37] K. Miyagawa, A. Kawamoto, Y. Nakazawa, and K. Kanoda, Phys. Rev. Lett. **75**, 1174 (1995).

[38] L. Balents, Nature (London) **464**, 199 (2010).